

## Chapter 2

# Contact Pressure of Total Ankle Replacement (TAR)

**Abstract** Three-dimensional (3D) models of a right ankle TAR have been created to represent Bologna-Oxford (BOX) TAR model. Finite element analysis of ankle stance phase of gait cycle was developed to simulate the static response behaviour and extract the data in determining the contact pressure on contact surface of the bearing and talar components. Sliding distance was determined by predominate motion of plantar/dorsi flexion of ankle stance phase gait cycle. Validity of contact analysis was conducted to make sure consistent, accurate, and therefore dependable procedures.

**Keywords** Contact pressure • Total ankle replacement • Finite element analysis • BOX • Sliding distance

## 2.1 Geometric Model

A three-dimensional (3D) model of a TAR was built using the computer-aided design (CAD) tool, SOLID WORKS. The BOX TAR was used throughout this simulation. The model of BOX TAR was chosen with regards to the shapes of the three components which were congruence with physiologic ankle mobility, the natural role of the ankle joint ligaments and encouraged early clinical result that demonstrated safety and efficacy [1, 2]. Figure 2.1 shows the dimensions of BOX TAR.

This model was developed to simulate the right ankle TAR. The metal parts of the tibial and talar components were assigned to be of Cobalt-Chromium (CoCr) material properties with titanium coating sprayed on articulating surfaces where the Young's modulus of 210 GPa and Poisson's ratio of 0.3 were applied to the model [3]. The tibial component with a spherical surface of 130 mm radius has contact with the bearing component which allows rotations [4]. The talar and bearing components have a concave sulcus of 35 mm radius where the bearing on the inferior surface is intact with talar components which is fully conformed to the bi-concave surface [5]. The thickness of the bearing varied in 1-mm increment from 5 to 8 mm [5]. The bearing component is ultra-high molecular weight polyethylene

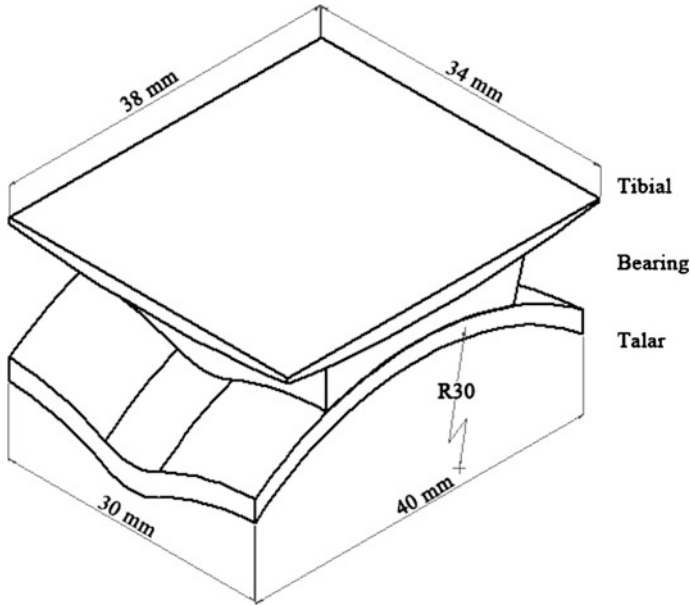


**Fig. 2.1** Implant geometry

(UHMWPE) material manufactured from compression moulded from GUR 1020 with Young's modulus of 500 MPa and Poisson's ratio of 0.3 [5].

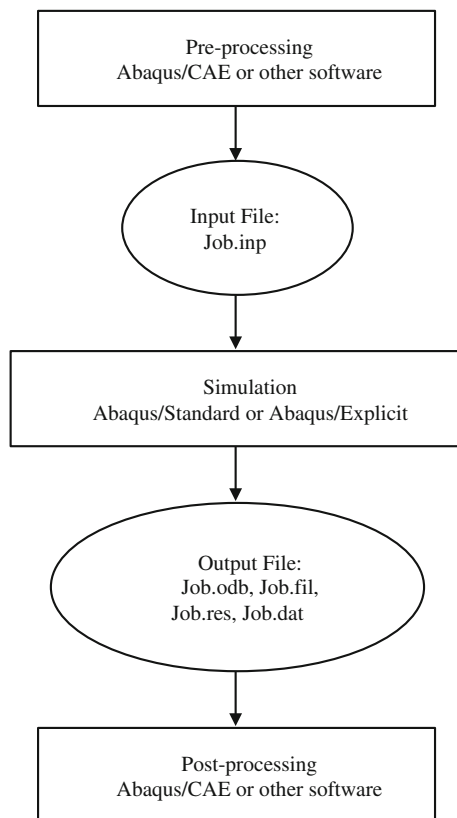
## 2.2 Finite Element Analysis

The finite element analysis is a numerical method to solve many problems in engineering and mathematical physics. The rapid development of computer technology encourages the use of finite element analysis as a method to solve various areas of problems. The utilization of finite element software is very useful for problems with complicated geometries, loading, and material properties, where analytical solutions are not available. Basically, there are three stages involving computer aided engineering (CAE) to complete the analysis [6]:

- i. Pre-processing—define the physical problem of the model included.
- ii. Simulation—background process that solves the numerical problem defined in the model.
- iii. Post-processing—evaluate the results obtained.

These three stages are linked together as shown in Fig. 2.2. This study on the development of computational wear prediction on total ankle replacement (TAR) was analysed using ABAQUS/CAE v6.09.

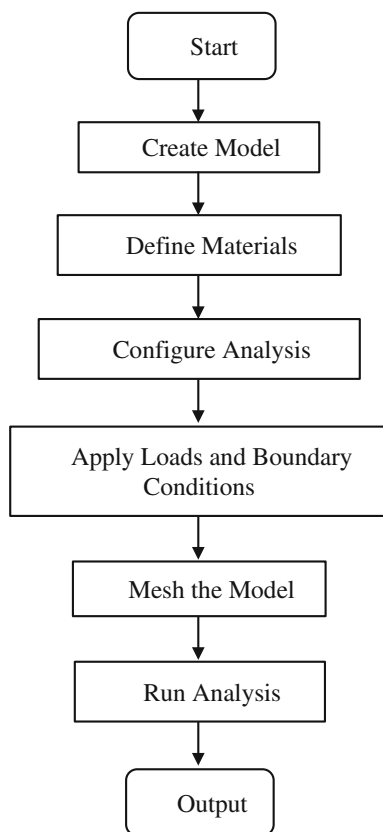
**Fig. 2.2** General analysis for finite element analysis [6]



### 2.2.1 Development of Finite Element Analysis of Gait Cycle

The finite element analysis is potential in making wear predictions. It is able to accurately consider both the variation of the loadings and the continuous change of the geometry caused by material removal in complex three-dimensional components. The computational simulation of wear prediction on total ankle replacement (TAR) simulated the static response behaviour of an ankle gait cycle which was conducted by using Abaqus/Standard. Wear prediction simulation used finite element analysis to extract the data in determining the contact pressure on contact surface of the bearing and talar components. The contact surface of the bearing and talar components were used to simulate wear because the sliding distance on contact surface of tibial and bearing components were relatively small (almost zero) and produce no wear. These reflect to the kinematics of ankle joint. The finite element analysis was used to visualize the wear prediction behaviour. The following steps in Fig. 2.3 simulate the BOX TAR model.

**Fig. 2.3** Flowchart of finite element analysis of gait cycle [6]



### 2.2.1.1 Create Model

The BOX TAR model consisted of three components which were tibial, bearing and talar. The details of this model geometry were explained in Sect. 2.1. The BOX TAR was modelled in SOLIDWORKS, a computer aided design (CAD) software. The model was converted to .SAT format which was compatible to the commercial ABAQUS software created in order to generate the model in the ABAQUS/CAE tool.

### 2.2.1.2 Define Materials

All components generated required the definition of the material properties. The Young's modulus and Poisson's ratio were defined in the property module of the ABAQUS/CAE software. The tibial and talar components were assigned to be of Cobalt-Chromium (CoCr) where the Young's modulus was 210 GPa and the Poisson's ratio was 0.3. The bearing component was assigned to be of ultra-high

molecular weight polyethylene (UHMWPE) where the Young's modulus was 500 MPa and the Poisson's ratio was 0.3.

### 2.2.1.3 Configure Analysis

In this simulation, the static responses were used. This is a single event that needed single analysis steps. Overall, the analysis consisted of two analysis steps where-by the ABAQUS/CAE generated an initial step automatically. The analysis step was created in the period of 0.625 s. The time period was determined by stance phase of time taken in the ankle gait cycle [7]. Stresses, displacements, and contact were requested in the field output while the energy was requested in the history output. All outputs requested for a whole model every 0.025 units of time. The output data required was contact pressure where by it was printed in the form of tables that was written in ABAQUS data (.dat) files.

The interaction was created using surface-to-surface contact, in which the contact property used was tangential behaviour. The friction coefficient between two articulating surfaces of the metal and bearing components were assumed to be 0.04 [8].

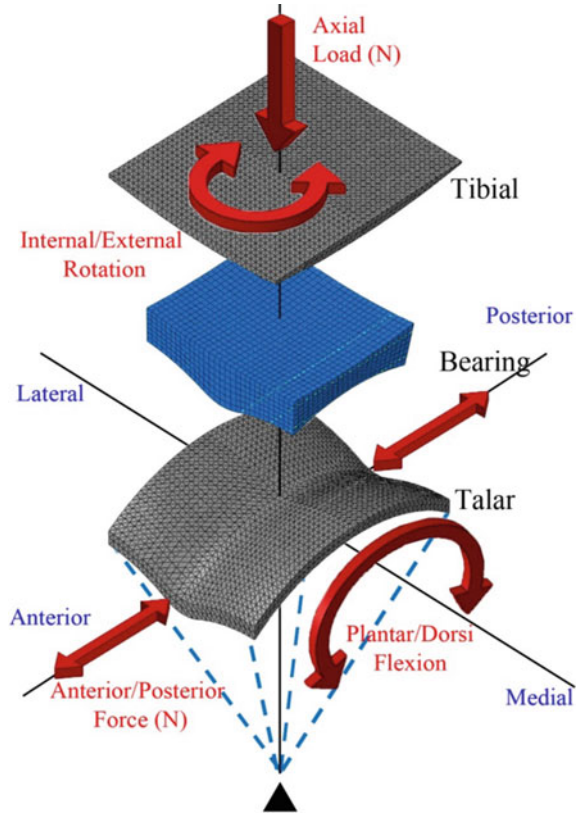
### 2.2.1.4 Apply Loads and Boundary Conditions

The tibial component was fixed in the distal tibia bone and the talar component was fixed at the articulating surfaces of the talar bone. In this simulation, the load created was an axial (vertical) load using concentrated force applied to the tibial component. The boundary condition of internal/external rotation was applied to the tibial component whereas the anterior/posterior force and plantar/dorsiflexion were applied to the talar component. The variation of load and boundary conditions of the stance phase of ankle gait cycle applied was utilized by creating tabular amplitude. The talar component was constrained using a tie at a point that was the center of articular surface of the talar dome as shown in Fig. 2.4. The applied boundary conditions and force predictions were based on previous work [9, 10]. Time histories of boundaries and force predictions of the stance phase of the gait cycle was considered to simulate wear predictions on the TAR model as shown in Fig. 2.5. The stance phase of gait cycle was divided into 25 instants.

### 2.2.1.5 Mesh the Model

There are hexa, wedge and tetra elements for the solid mesh element available in ABAQUS/CAE. Tetrahedral elements are geometrically versatile and used in many automatic meshing algorithms. It is very easy to mesh a complex shape with tetrahedral elements. It is known as a robust element and occasionally used as a rigid element. The hexahedral elements normally provide a good mesh with a

**Fig. 2.4** Load and boundary conditions configuration on finite element simulation model



solution of equivalent accuracy at less cost. However, tetrahedral elements are less sensitive to initial element shape, whereas first-order hexahedra perform better if their shape is approximately rectangular.

The metal parts of the tibial and talar components were modelled as four nodes which were three-dimensional tetrahedral elements represented as rigid triangles. The number of elements was 36,457 and 16,224 respectively. The tetrahedral element was stiffer than the hexahedral element. This was due to more points of integration in the hexahedral element than the tetrahedral element. Thus, the tibial and talar components, as hard parts, were assigned to use the tetrahedral element while the UHMWPE bearing was assigned to use 5760 element of eight node hexahedral elements as soft part.

### 2.2.1.6 Run Analysis

After having configured the analysis, a job was created and submitted for analysis. The input analysis generated the input files and analysed the model. Then, the

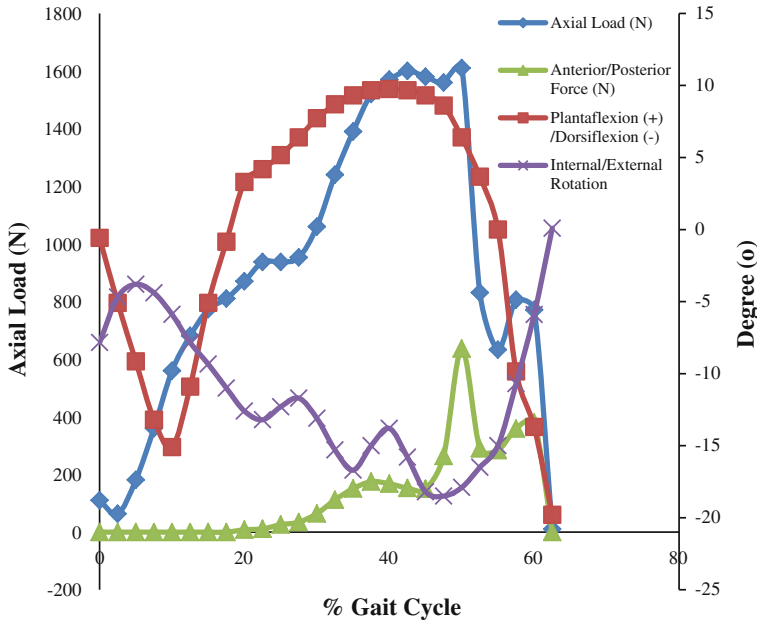


**Fig. 2.5** Time histories of applied boundary conditions and force predictions of stance phase

results of the completed analysis were visualized by using the ABAQUS/CAE under the visualization module.

### 2.3 Contact Analysis

Contact analysis is crucial to determine the contact area and contact pressure of the wear model. Figure 2.6 shows geometrical characteristic to define an analytical model of contact analysis. It was calculated using the Hertzian theory for elastic contact of two bodies with non-conforming geometrical shapes. However, another researcher improved mathematical formulation for a case of a sphere in contact inside a sphere [11].

The contact analytical model began with the local contact pressure model,  $\sigma_t(\theta, \phi)$  calculated as follows:

$$\sigma_t(\theta, \phi) = \frac{3W(t)}{2\pi r^2(t)} \left[ 1 - \frac{d_t^2(\theta, \phi)}{r^2(t)} \right]^{1/2} \quad (2.1)$$

where  $r(t)$ , which is the radius of the surface contact edge, is given by

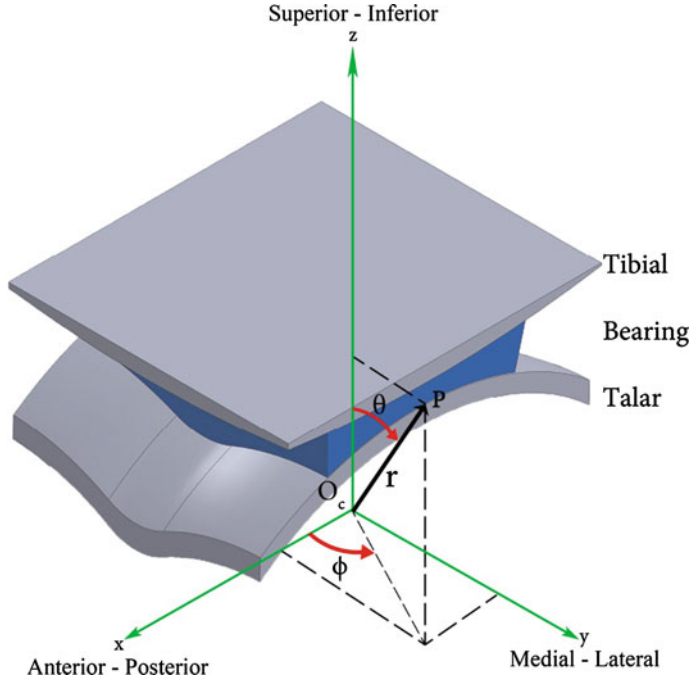


**Fig. 2.6** Geometrical characteristic of TAR model: anatomical directions

$$r(t) = \left[ \frac{3\pi}{8} W(t) \left( \frac{1 - \nu_h^2}{\pi E_h} - \frac{1 - \nu_c^2}{\pi E_c} \right) \left( \frac{1}{D_h} - \frac{1}{D_c} \right)^{-1} \right]^{1/3} \quad (2.2)$$

where  $W(t)$  is the axial load,  $D_h$  is the talar component diameter,  $D_c$  is the meniscal bearing diameter,  $E_h$  is the Young's modulus of CoCr,  $E_c$  is the Young's modulus of UHMWPE,  $\nu_h$  is the Poisson ratio of CoCr, and  $\nu_c$  is the Poisson ratio of UHMWPE.  $d_t(\theta, \phi)$  is the distance from the contact surface of axial load to the generic point P (node) [11].

### 2.3.1 Contact Pressure of Total Ankle Replacement (TAR)

The compressive forces during gait that acted on the ankle joint that transferred from the knee joint will result as contact pressure. The magnitude and distribution of contact pressure is important, where it can affect the wear rates of ankle replacement and for severe conditions can lead to fracture of polyethylene. The geometry and features of the artificial ankle are very important to determine the



**Table 2.1** Contact pressure of TAR

Source	Implant	Load (N)	Type of study	Peak contact pressure (MPa)
Regianni et. al. (2006) [12]	BOX	1600	FEM	16.1
Miller et. al. (2004) [13]	Agility	3330	FEM	25
Nicholson et. al (2004) [14]	Agility	700	Tekscan	21.2
Fukuda et. al. (2010) [15]	Agility	740	Tekscan	5.7
McIff et. al. (2001) [16]	STAR	3650	FEM	8-10

contact pressure. The conformity between metal components such as polyethylene and thickness of polyethylene are elements that can affect the contact pressure.

Several studies have been conducted using different methods to resolve the contact pressure on particular total ankle replacement. It has been reviewed that the predicted or measured contact pressure in existing implants are inconstant due to different methodologies and implant geometry. The reported contact pressures are between 5.7 and 25 MPa. These stresses have been recorded from clinically successful designs. The tabulated contact pressures from previous studies are demonstrated in Table 2.1.

## 2.4 Sliding Distance

The computational simulation of ankle replacement was predominated by plantar/dorsi flexion motion. The plantar flexion and dorsi flexion is the major contributor to total ankle motion. The average range of motion (ROM) of plantar flexion and dorsiflexion of the ankle was measured at 40°–56° and 13°–33°, respectively [17]. Therefore, the sliding distance was considered by calculation based on the plantar/dorsi flexion motion whereby the point on the surface slides against the interacting surfaces between the bearing and talar interface used in the calculation. The sliding distance was approximated by the arc length between the two points with the change of an angle:

$$s_i(\theta, \phi) = \Delta\eta_i r(\theta, \phi) \quad (2.3)$$

where  $\Delta\eta_i$  is the difference in the plantar/dorsi flexion of angle and  $r(\theta, \phi)$  is the perpendicular distance between a point on the bearing and talar interfaces and the rotation of plantar/dorsi flexion axis. The difference in angle of plantar/dorsi flexion was determined from mid-position of previous intervals to the mid-position of the successive interval that gave by:

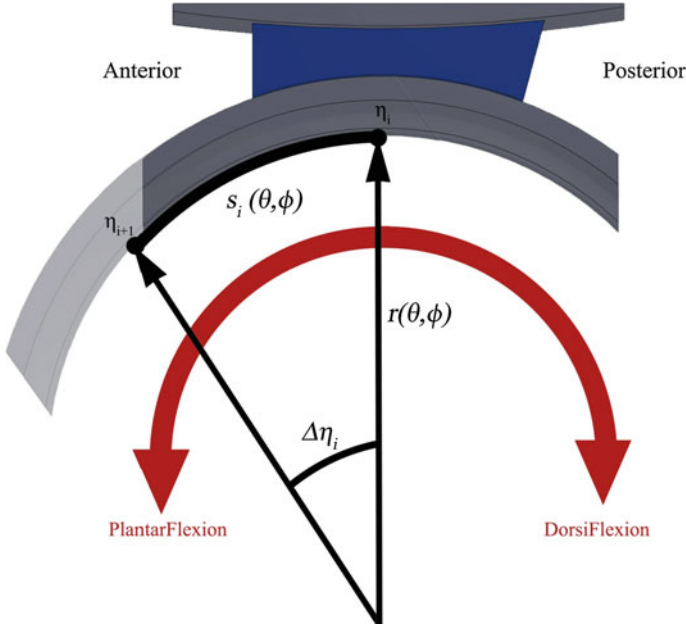


**Fig. 2.7** Schematic of the sliding distance using plantar/dorsi flexion angles

$$\Delta\eta_i = [\eta_i + \eta_{i+1} - \eta_{i-1}/2] - [\eta_{i-1} + \eta_i - \eta_{i-1}/2] = (\eta_{i+1} - \eta_{i-1})/2 \quad (2.4)$$

where  $\eta_{i-1}$  is the previous interval,  $\eta_i$  is the current interval, and  $\eta_{i+1}$  is the successive interval. The schematic diagram of sliding distance calculation is illustrated in Fig. 2.7 [18].

## 2.5 Validity of Contact Analysis

The purpose of validation is to ensure the validity of methodology and that the procedures used for the development of computational wear simulation on total ankle replacement (TAR) are consistent, accurate, and therefore dependable. The direct correlations of the present wear simulation using computational method and the previous works of wear simulation using a simulator are difficult to handle due to fairly limited resources found on studies of the BOX TAR. However, there are different total ankle replacement designs (other type of ankle implant) that have been analysed with different loading and boundary conditions that have been used to further strengthen findings of the present study.

2.5.1 Mesh Sensitivity Test

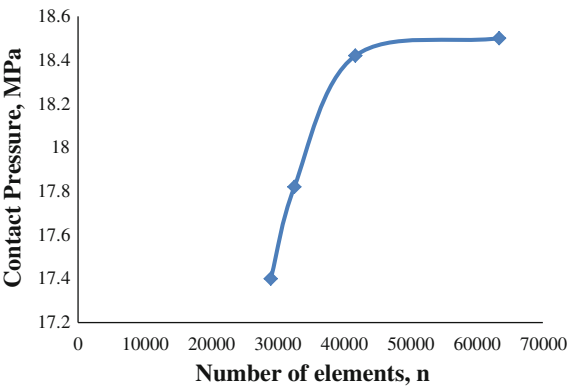
The mesh convergence test was performed at the edge of the meniscal bearing surface contact anteriorly. The details are in Table 2.2.

Generally, in finite element modelling, mesh sensitivity analysis was carried out to determine the optimum size of mesh for the study. Usually, a finer mesh typically results in a more accurate solution. Factually, it was agreed with the principal behaviour of finite element that the number of elements were directly proportional to the time taken to complete a certain analysis. When mesh sizes reduced, the number of elements increased while the contact pressure increased. As shown in Fig. 2.8, the effects of meshing were converged at the mesh sizes of 1.0 and 0.9 mm. As the mesh size of 0.9 mm was used, the time taken to complete a single wear cycle was about 40 min which was almost double from the mesh size of 1.0 mm, in which the time taken was about 23 min. It was very difficult to compare contact pressure from experimental tests, because the previous works on wear that particularly used BOX TAR did not mention about the contact pressure obtained using a simulator. In fact, they did mention to use the contact pressure based on the study using finite element analysis [7, 12]. Therefore, throughout the study 1.0 mm was used.

Table 2.2 Mesh sensitivity details

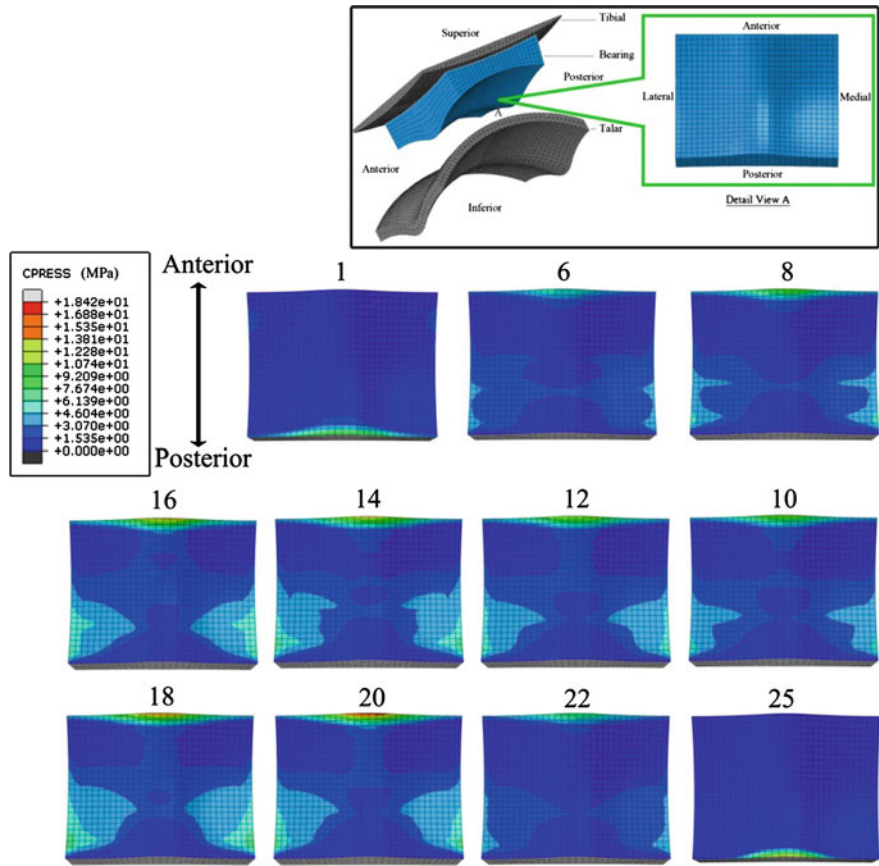
Mesh size (mm)	No. of elements	Maximum contact pressure (MPa)	Time taken (min)
1.2	29,019	17.4	13
1.1	32,576	17.82	17
1.0	41,748	18.42	23
0.9	63,418	18.5	40

Fig. 2.8 A plot of maximum contact pressure versus number of elements, n shows the changes in contact pressure for the different mesh densities



2.5.2 Contact Analysis

It has been addressed in the previous study that the maximum contact pressure experienced by the talar component was 16.1 MPa at 79 % of stance phase [12]. The region of maximum contact pressure was observed in the medial region of 75 % of dorsiflexion. In this study, the maximum contact pressure was 18.4 MPa at 79 % of the stance phase of the 20th instant at the tip of the anteriorly region of the meniscal bearing as demonstrated in Fig. 2.9. A difference of 14 % between these two results therefore revealed that the value of this study has agreement with the one found in the previous study. The most contacted area experienced less than 10 MPa. The contact pressure based on the Hertzian’s theory of modified mathematical formulation was about 10.56 MPa. It shows the difference between the previous study and the present study. The difference could be due to the limitation



**Fig. 2.9** Contact pressure distributions of the bearing contact surface between bearing-talar contacts for selected instant of stance phase of gait cycle

of the geometry simplification in Hertzian's theory and the geometry of TAR. The maximum contact pressure in this present study indeed shows in the range from previous studies (5.7–25 MPa) as shown in Table 2.1.

It is also important to mention that the model used in this study was not in consideration of the ligamentous structure. This was due to the fact that the mechanism simulated here was practically replicating the joint simulator, in which the external loading applied throughout the analyses.

It was also found in this study that the wear phenomenon occurred at the anterior tip of the meniscal bearing, whereas previous studies have demonstrated contradiction [12]. This was believed to occur due to different loading and movement conditions. This study allowed anterior/posterior displacement together with rotation whereas the previous study restricted the movement of the implant to consider the rotation alone (plantar/dorsi flexion) [19, 20]. The full triaxial was implemented in this study to simulate the physiological ankle activity. The settings used in this study were supported by findings whereby the contact pressures between the meniscal bearing and talar component were within the physiological value as found in the previous study [7].

## References

1. Vickerstaff Ja, Miles AW, Cunningham JL (2007) A brief history of total ankle replacement and a review of the current status. *Med Eng Phys* 29:1056–1064
2. Leardini a, O'Connor J, Catani F, Romagnoli M, Giannini S (2008) Preliminary results of a biomechanics driven design of a total ankle prosthesis. *J Foot Ankle Res* 1:08
3. Wang FC, Jin ZM, McEwen HMJ, Fisher J (2003) Microscopic asperity contact and deformation of ultrahigh molecular weight polyethylene bearing surfaces. *Proc Inst Mech Eng Part H J Eng Med* 217:477–490
4. Ianuzzi A, Mkandawire C (2006) Applications of UHMWPE in total ankle replacements, 2nd edn. *UHMWPE biomaterials handbook*. doi:[10.1016/B978-0-12-374721-1.00011-0](https://doi.org/10.1016/B978-0-12-374721-1.00011-0)
5. Leardini A, O'Connor JJ, Catani F, Giannini S (2004) Mobility of the human ankle and the design of total ankle replacement. *Clin Orthop Relat Res* 424:39–46
6. Simulia DS (2012) Getting Started with Abaqus: Interactive Edition (6.12). p 695
7. Affatato S, Leardini a, Leardini W, Giannini S, Viceconti M (2007) Meniscal wear at a three-component total ankle prosthesis by a knee joint simulator. *J Biomech* 40:1871–1876
8. Godest aC, Beauginon M, Haug E, Taylor M, Gregson PJ (2002) Simulation of a knee joint replacement during a gait cycle using explicit finite element analysis. *J Biomech* 35:267–275
9. Seireg A, Arvikar RJ (1975) The prediction of muscular load sharing and joint forces in the lower extremities during walking. *J Biomech* 8:89–102
10. Stauffer RN, Chao EY, Brewster RC (1977) Force and motion analysis of the normal, diseased, and prosthetic ankle joint. *Clin Orthop Relat Res* 127:189–196
11. Raimondi MT, Santambrogio C, Pietrabissa R, Raffelini F, Molfetta L (2001) Improved mathematical model of the wear of the cup articular surface in hip joint prostheses and comparison with retrieved components. *Proc Inst Mech Eng Part H J Eng Med* 215:377–390
12. Reggiani B, Leardini a, Corazza F, Taylor M (2006) Finite element analysis of a total ankle replacement during the stance phase of gait. *J Biomech* 39:1435–1443
13. Miller MC, Smolinski P, Conti S, Galik K (2004) Stresses in polyethylene liners in a semiconstrained ankle prosthesis. *J Biomech Eng* 126:636

14. Nicholson JJ, Parks BG, Stroud CC, Myerson MS (2004) Joint contact characteristics in agility total ankle arthroplasty. *Clin Orthop Relat Res* 424:125–129
15. Fukuda T, Haddad SL, Ren Y, Zhang L (2010) Impact of talar component rotation on contact pressure after total ankle arthroplasty: a cadaveric study. *Foot Ankle Int* 31(5):404–411
16. McIff TE, Saltzman C, Brown T (2011) Contact pressure and internal stresses in a mobile bearing total ankle replacement. In: 45th annual meeting of the orthopaedic Research Society, San Francisco, CA, pp 25–28
17. Lundberg A, Goldie I, Kalin BSG (1989) Kinematics of the ankle/foot complex—Part 1: Plantarflexion and dorsiflexion. *Foot Ankle* 9:194–200
18. Maxian TA, Brown TD, Pedersen DR, Callaghan JJ (1996) 3-Dimensional sliding/contact computational simulation of total hip wear. *Clin Orthop Relat Res* 333:41–50
19. Bell CJ, Fisher J (2006) Simulation of polyethylene wear in ankle joint prostheses. *Biomed Mater Res B Appl Biomater* 81:162–167
20. Grosland M PhD, Pedersen DR, Thomas TP (2008) Analysis as a metric of degeneration propensity. *Biomech Model Mechanobiol* 5:82–89

Wear Prediction on Total Ankle Replacement

Effect of Design Parameters

Saad, A.P.B.M.; Syahrom, A.; Harun, M.N.; Kadir, M.R.A.

2016, XIII, 55 p. 41 illus., 35 illus. in color., Softcover

ISBN: 978-3-319-21722-2